Microstructural, chemical and textural characterization of ZnO nanorods synthesized by aerosol assisted chemical vapor deposition.

A. Sáenz-Trevizo, P. Amézaga-Madrid, L. Fuentes-Cobas, P. Pizá-Ruíz, W. Antúnez-Flores, C. Ornelas-Gutiérrez, S. A. Pérez García, M. Miki-Yoshida.

Abstract

ZnO nanorods were synthesized by aerosol assisted chemical vapor deposition onto TiO_2 covered borosilicate glass substrates. Deposition parameters were optimized and kept constant. Solely the effect of different nozzle velocities on the growth of ZnO nanorods was evaluated in order to develop a dense and uniform structure. The crystalline structure was characterized by conventional X-ray diffraction in grazing incidence and Bragg–Brentano configurations. In addition, two-dimensional grazing incidence synchrotron radiation diffraction was employed to determine the preferred growth direction of the nanorods. Morphology and growth characteristics analyzed by electron microscopy were correlated with diffraction outcomes. Chemical composition was established by X-ray photoelectron spectroscopy. X-ray diffraction results and X-ray photoelectron spectroscopy showed the presence of wurtzite ZnO and anatase TiO_2 phases. Morphological changes noticed when the deposition velocity was lowered to the minimum, indicated the formation of relatively vertically oriented nanorods evenly distributed onto the TiO_2 buffer film. By coupling two-dimensional X-ray diffraction and computational modeling with ANAELU it was proved that a successful texture determination was achieved and confirmed by scanning electron microscopy analysis. Texture analysis led to the conclusion of a preferred growth direction in [001] having a distribution width $\Omega=20° \pm 2°$.

Kewords: ZnO nanorods, Texture determination, 2D X-ray diffraction, ANAELU software, Electron microscopy.

Introduction

ZnO iswell known as a versatile material. According to the literature, it is suitable for a wide range of applications, i.e. solar cells, gas sensors and photocatalyst [1–11]. As a consequence of its two polar surfaces and thirteen fast growth directions, ZnO can be easily obtained in various morphologies including nanorods, nanowires and nanotubes [4,5,10]. Among its multiple configurations, one-dimensional (1D) structures in the form of nanorods are of great interest. Using this 1D morphology a larger surface to volume ratio is provided, increasing the amount of active material for a specific surface process. This effect can make it convenient for a major variety of purposes [1,3–15].

The synthesis of highly oriented 1D structure favoring a crystalline orientation (texture) is in some cases a desired characteristic for a particularmaterial. The later, own to a contribution in the rise of its performance [3,4,6,8,9,14]. In agreementwith various reports, the development of well-ordered ZnO nanorod arrays can be achieved by first growing a layer of seeds that serve as effective nucleation sites. An alternative method is to use a crystalline substrate, where ZnO rods can be later deposited [1–13]. Both routes have demonstrated the possibility to generate uniform hexagonal c-axis oriented nanorods, from which the texture estimation has been expressed in terms of X-ray diffraction observations or through the calculation of the Lotgering factor [1,2,9,11]. However, neither one of the two methods represents a complete definition of the degree of orientation of the material. This, as only the analysis of the measured intensities is

comprised [1,15]. Nonetheless, these approaches can be employed as an acceptable approximation to describe the preferred growth direction of the analyzed structure.

These works focus in the synthesis, detailed microstructural characterization and accurate texture determination of a ZnO nanorod layer deposited over a TiO_2 film covered borosilicate glass substrates (BSG). The whole structure was grown by aerosol assisted chemical vapor deposition technique (AACVD). Several techniques were used to perform the detailed microstructural characterization and textural analysis; X-ray diffraction (conventional and synchrotron radiation) and electron microscopy, were included. Results were complemented with computationalmodeling in order to quantitatively establish the orientation of the nanorods.

Materials and methods

Synthesis of nanostructures: ZnO nanorods were deposited by AACVD technique with a configuration similar to that previously reported elsewhere [16,17]. The nanorod layer was synthesized onto TiO_2 thin film covered borosilicate glass substrates of 2.5 × 2.5 cm^2. For TiO_2 layer deposition, the concentration of the starting solution was 0.05 $mol \cdot dm^{-3}$ of titanium(IV) oxyacetylacetonate (90%) in methanol (99.8%). Precursor solution concentration for ZnO was 0.1 $mol \cdot dm^{-3}$ of zinc chloride (97%) in tridistilledwater. In this case, the addition of small amounts of hydrochloric acid (37%)was needed to completely dissolve the solute, resulting in a final HCl concentration of 6 $mmol \cdot dm^{-3}$.

Optimumdeposition conditions of eachmaterial depend principally on precursor solution composition (solute and solvent) and the desired microstructural characteristics. In thiswork, the TiO_2 layerwas deposited as a buffer, to prevent diffusion

from glass substrate, therefore we needed a smooth and uniform layer. Consequently to deposit it, a surface kinetic limited growth mechanismwas generated using a lower deposition temperature and concentration (0.05 mol·dm^{-3}); however, since a crystalline or polycrystallinematerial performs as a better diffusion barrier, than an amorphous layer, the deposition temperature should not be excessively low. Then 673±1 Kwas employed for the deposition of TiO_2 layer. In contrast, the ZnO nanorod layer was promoted by a transport limited mechanism; where growth direction was towards the precursor gradient near from the substrate surface. Accordingly a higher deposition temperature of 823 ± 1 K and concentration (0.1 mol·dm^{-3})were set for ZnO nanorod. The scan velocity of the nozzlewas selected according to the synthetized layer: for TiO_2 layer it was kept at 6.6 10^{-3} cm·s^{-1} and in order to obtain a uniform layer of ZnO nanorods, it was varied from 16.6 10^{-3} to 3.3 10^{-3} cm·s^{-1} at intervals of 3.3 10^{-3} cm·s^{-1}. Microfiltered air at 318 ± 1 K was used as carrier gas, with a flux of 8 and 5 dm^3·min^{-1} for deposition of TiO_2 and ZnO layers, respectively.

Characterization: Conventional grazing incidence X-ray diffraction (GIXRD) patterns were performed to determine the crystalline phases of the bilayered materials, using a PANalytical X-Pert systemworkingwith a Cu Kα radiation (λ= 0.1542 nm) at 40 keV and 30 mA. The grazing angle was set at 0.5° and the scanning angle 2θ was varied between 20° and 80° at 0.05° step. Bragg–Brentano X-ray diffraction experiment was also carried out under similar conditions (radiation source, scanning angle range and step size). Selected sample having nanorods evenly distributed on the surface was investigated by two-dimensional grazing incidence synchrotron diffraction (2D-GIXRD) at beamline 11-3 of Stanford Synchrotron Radiation Lightsource. The parameters used

for this study were: X-ray wavelength of 0.0974399 nm; 2D-detector mar345 (diameter 345 mm); sample to detector distance of 125 mm; screen pixel dimensions of 0.15 × 0.15 mm^2 and grazing incidence angle of 0.1°. The experimental Debye rings were processed with the FIT2D software [18], followed by its simulation with ANAELU [19,20] in order to analyze the sample's texture. The aimto analyze the crystalline structure applying different X-ray diffraction methods was to obtain complementary information about textural properties of the developed material.

Surface morphology of the samples was studied by field emission scanning electron microscopy (SEM) in a JEOL JSM-7401F. Microstructural analysis of the samples was accomplished by high-resolution transmission electron microscopy (HRTEM) in a JEOL JEM-2200FS+Cs equipped with a spherical aberration corrector in the condenser lens and operated at an accelerating voltage of 200 kV. Selected area electron diffraction patterns (SAED) were also employed in the microstructural characterization. In order to perform HRTEM analysis, material from the as deposited sample was directly scratched from the substrate, dispersed in methanol and later placed on a TEM grid. The optical properties were determined from total reflectance and transmittance spectra in the UV–VIS–NIR interval in a CARY 5000 Spectrophotometer. Chemical composition and bond configuration were analyzed by X-ray photoelectron spectroscopy (XPS) on a Thermo Scientific Escalab 250Xi instrument. The photoelectron source was AlKα (1486.68 eV) X-ray using a monochromator with a spot size of 650 μm. Operating pressure was ~10^{-10} mbar.

Results and discussion

Crystalline structure, texture analysis and microstructure: According to GIXRD patterns in Fig. 1(a) it was concluded that all samples were polycrystalline. Observed peaks at about 25.2, 48.1 and 55.0 degrees fitted, respectively the (101), (200) and (211) family planes of TiO_2 as anatase (PDF 021-1272 [21]). Remaining peaks matched with diffracting lines of ZnO as wurtzite (PDF 01-075-1533 [22]). An increase in peak intensity and a decrease in peak broadening were noticed when the nozzle scan velocity employed to deposit the ZnO layer, was lowered. These changes can be attributed to the deposition of increased quantities of material (more intensity) and to the formation of larger crystals (less broadening). The appearance of a noteworthy peak intensity at $2\theta \cong 34.4°$, assigned to ZnO (002) planes, indicates some preferential growth orientation of the nanorods; consistent with the low intensity of {100} planes (as discussed below). Additional X-ray diffraction analysis with the aim to confirm such preferential growth, was performed under Bragg–Brentano configuration for sample TZ3 obtained at 3.3 10^{-3} $cm \cdot s^{-1}$ (Fig. 1(b)). Results indicated that most of the recorded peaks collected in GIXRD were also detected and corresponded to the previously identified phases. Peak at around $2\theta \cong 34.4°$ was again visible and significantly intense, confirming some preferential growth orientation of the nanorods around the normal to the substrate. Combined consideration of both studies suggested the presence of a significant number of nanorods having its axis inclined at $\gamma \cong 17.17°$ to the normal of the substrate's surface and other important amount of nanorods, exhibiting its axis normal to the substrate's surface.

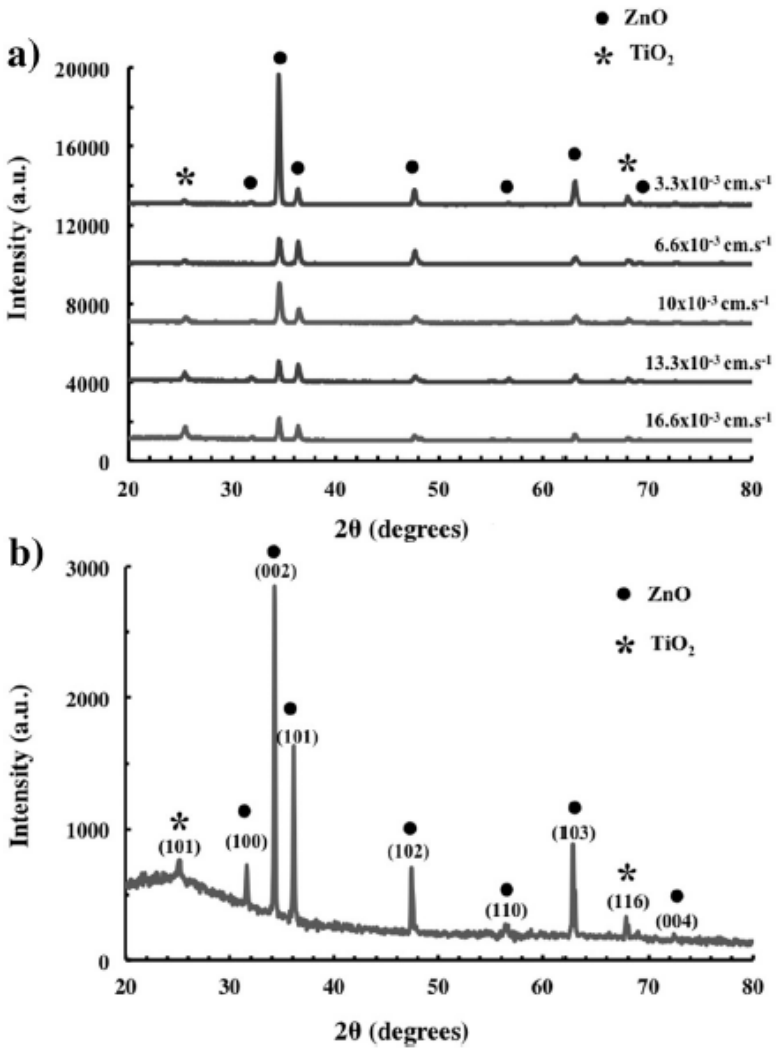

Fig. 1. X-ray diffraction patterns obtained by: a) GIXRD and b) Bragg–Brentano configuration. The pattern in a) shows the crystallographic composition of the samples and the presence of ZnO as wurtzite and TiO_2 as anatase phases, while pattern in b) was obtained in order to set differences between both techniques.

This conclusion resulted fromthe intense detection of peak for (002) planes under both experimental configurations, which denotes the development of an organized structurewith relatively vertically oriented nanorods. Representations of Bragg–Brentano and grazing incidence arrangements are shown in Fig. 2(a and b),where the Bragg condition for (002) planes in both arrangements is illustrated.

Resulting 2D-GIXRD pattern as obtained at the SSRL beamline 11-3 for sample TZ3 appears in Fig. 3(a). The modulation of intensities along the Debye rings, significantly those of (100) and (002) planes, indicates the existence of a considerable preferred orientation, as detected in GIXRD and Bragg–Brentano measurements. Semi-quantitative texture analysis of the ZnO phase in sample TZ3 was performed by modeling proposed inverse pole figures and associated 2D-GIXRD by application of ANAELU program. Crystallographic data of ZnO was taken from ICSD file 180052. Best qualitative fitting between modeled and experimental patterns was obtained considering a fiber texture, formed by a Gaussian distribution of the [001] crystal direction perpendicular to the sample's surface, with a distribution width Ω=20 ± 2°. The following expression represents the considered inverse pole figure:

$$R(\phi) = Ae^{-\left(\frac{180\phi}{\pi\Omega}\right)^2}.$$

Parameter A is fitted by ANAELU to satisfy required normalization conditions. For the optimized distribution breadth (Ω = 20°) it is found that A= 33.5. Simulated 2D-GIXRD pattern employing the previous outcomes appears in Fig. 3(b), which can be compared to experimental 2D-GIXRD in Fig. 3(a). A clear correspondence of ring position and distribution can be noted within both graphics, showing a successful texture determination. Comparison with results of pole figure conventional texture analysis of Pung et al. [23] shows a clear coincidence with samples synthesized by ALD at 280 °Cwith dominant [001] crystal axis oriented perpendicular to the substrate.

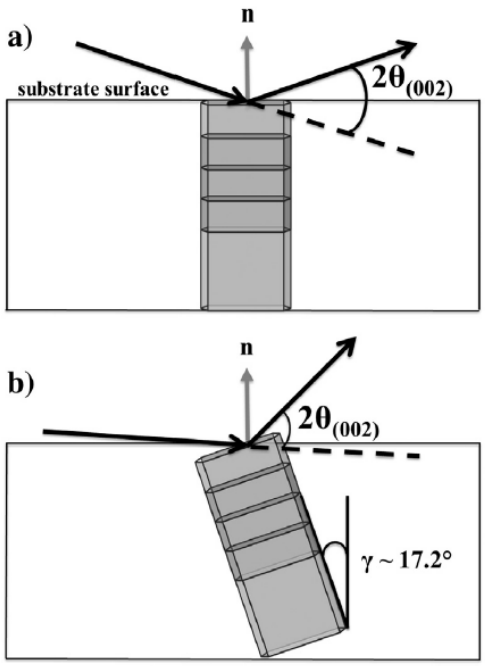

Fig. 2. Geometrical configuration reached during X-ray diffraction experiments. Illustrations correspond to: a) Bragg–Brentano and b) grazing incidence configurations.

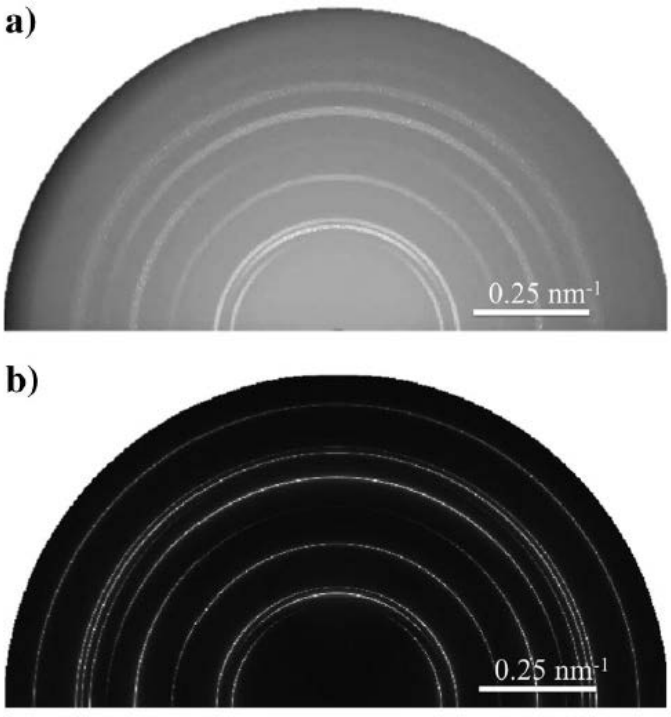

Fig. 3. 2D-GIXRD patterns of ZnO nanorods: a) as observed at SSRL and b) showing the texture simulation with *ANAELU*.

An alternative route used for texture description which is often found in the literature, adopts the so-called Lotgering factor [2,9]. In the present work, it is preferred to work with the (inverse and direct) pole figures for quantitative characterization of texture, following references [1,15]. Pole figures are integrated parts of the ANAELU software and so, served as a tool to compare experimental and simulated patterns.

Scanning electron micrographs in Fig. 4 show that in all cases, nanorods in the form of polygonal and columnar structures were developed onto TiO_2 film. According to SEMresults, itwas evident that a more uniform distribution of nanorods covering the substrate (case of TZ3 sample) took place when the nozzle scan velocity was diminished to 3.3 10^{-3} $cm \cdot s^{-1}$, i.e. lesser uncovered zoneswere observedwhen reducing the velocity. As suggested in X-ray analysis, the formation of wider nanorods accompanied a more uniform coverage and distribution of the material on the substrate.

Cross sectional SEMmicrograph (see Fig. 5(a)) showed the presence of a very thin (~50 nm) TiO_2 filmthat behaved as a source of nucleation sites for nanorod growth as well as a buffer film to prevent diffusion of Na and Si, from substrate to the nanostructures. This film was well adhered and uniformly distributed on the borosilicate substrate, having a thickness of about 50 nm in all samples. Cumulative results depicted so far, supported the election of sample TZ3 for full characterization. Complementary examination of sample TZ3 using cross sectional SEM micrographs, served to confirm nanorod orientation and its mean inclination fromthe normal of the substrate.Within micrographs, itwas noticed that many nanorods grew vertically oriented and some others, appeared at a certain inclination from the perpendicular to the substrate; fact that matches with the deductions of sample's texture from X-ray

diffraction analysis. Fig. 5(a) shows a representative image, from where the average nanorods' axis inclination was computed. As a result of several measurements (106 structures), a mean inclination of −4 ± 23° was determined (clockwise direction +). Fig. 5(b) presents the distribution of ZnO nanorod axis inclination surrounding the substrate normal; it is shown that a distribution centered around 0° slightly shifted to negative angles. This result served to support the crystallographic observations presented previously in the X-ray diffraction analysis; these measurements were possible because each nanorod can be analyzed separately. The latter observations proved that the texture analysis performed herein was suitable for accurate 1D structure orientation definition. In the case of Ariosa et al. [1], the morphological and geometrical characteristics of the nanorods were also helpful for the texture determination. Furthermore, 2D-GIXRD was also applied to thin films, according to the work presented by Ramos-Cano et al. who characterized $PbTiO_3$ [24].

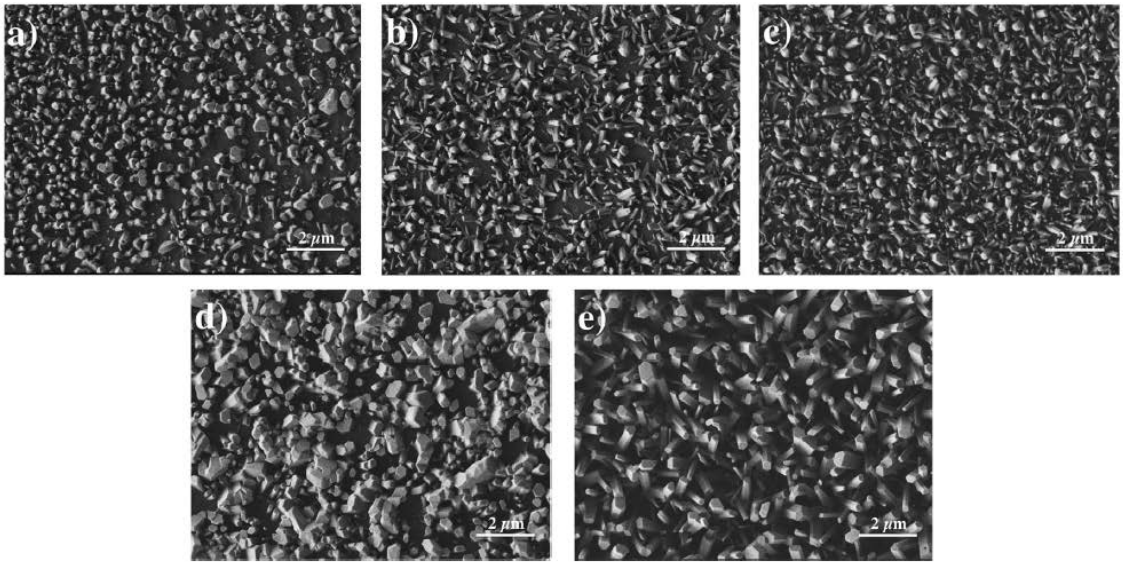

Fig. 4. Formation of ZnO nanorods deposited at: a) 16.6, b) 13.3, c) 10 d) 6.6 and e) 3.3×10^{-3} cm·s^{-1} (sample TZ3).

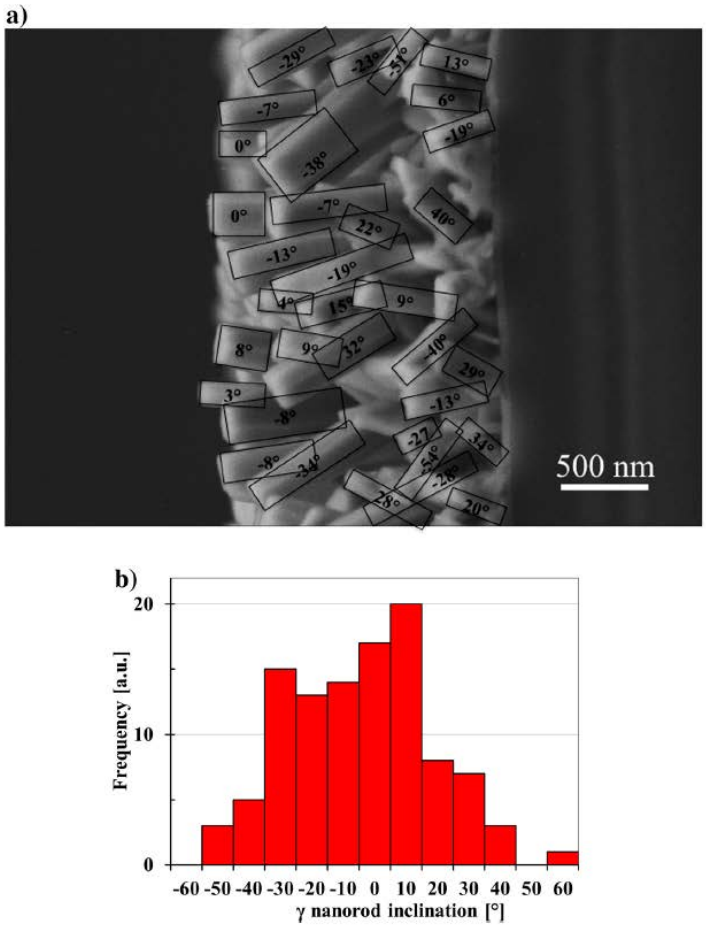

Fig. 5. a) SEM micrograph of textured sample TZ3 obtained in cross section. Image exhibits several ZnO nanorods and their axis inclination from substrate normal. b) Inclination distribution of ZnO nanorod axis around substrate normal.

An HRTEM micrograph obtained for nanorod of sample TZ3 confirmed that each columncorresponded to a single crystal, having its longitudinal axis developed along the [001] direction. This fact was deduced from the measurement of the lattice fringes in Fig. 6. Fig. 6(a) shows lattice fringes of 0.263 ± 0.003 nm consistent with (002) family planes; the inset shows a general view of the nanorod. In Fig. 6(b) it is shown an atomic resolution images obtained by fast Fourier transform processing of the squared region signaled in Fig. 6(a); a clear disposition of lattice fringes (planes) transversal and parallel to the axial direction of the nanorod were noticed. Lattice fringes of 0.263 ± 0.003 nm and 0.167 ± 0.002 nm, consistent with (002) and (110) family planes,

respectively were quantified. It corroborates the nanorod orientation, with its longitudinal axis parallel to the reciprocal lattice vector $g_{(002)}$ and transversal direction parallel to $g_{(110)}$; the inset shows the indexed SAED pattern that confirms the nanorod orientation. Calculated lattice parameters of a = 0.333 ± 0.003 nm and c = 0.526 ± 0.005 nm, were in good agreement with crystallographic information of ZnO (PDF 01-075-1533 [22]).

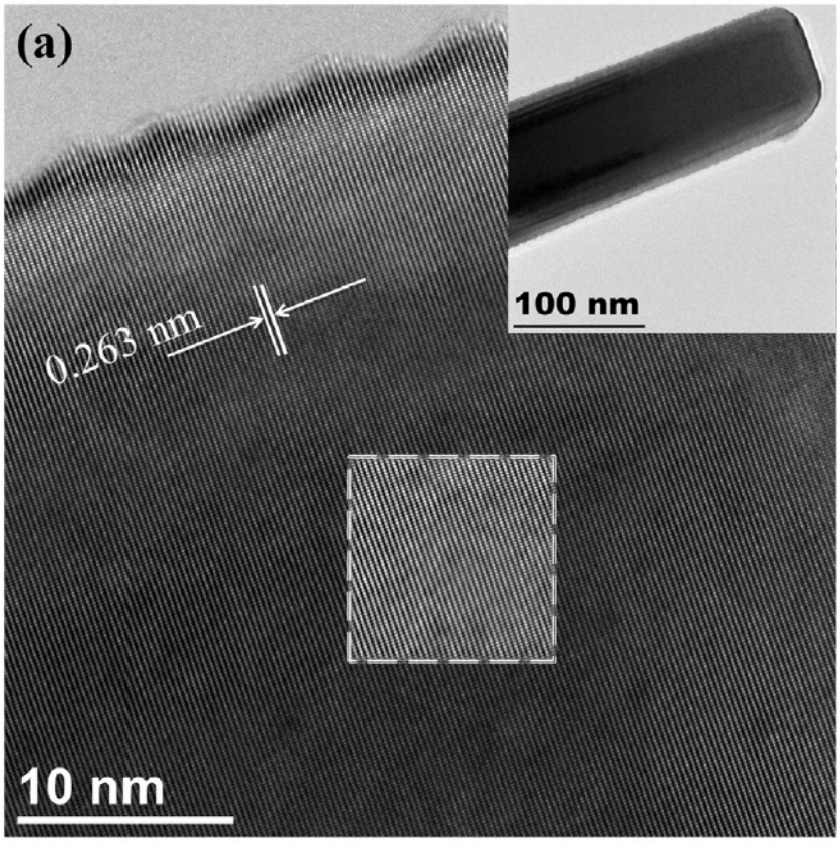

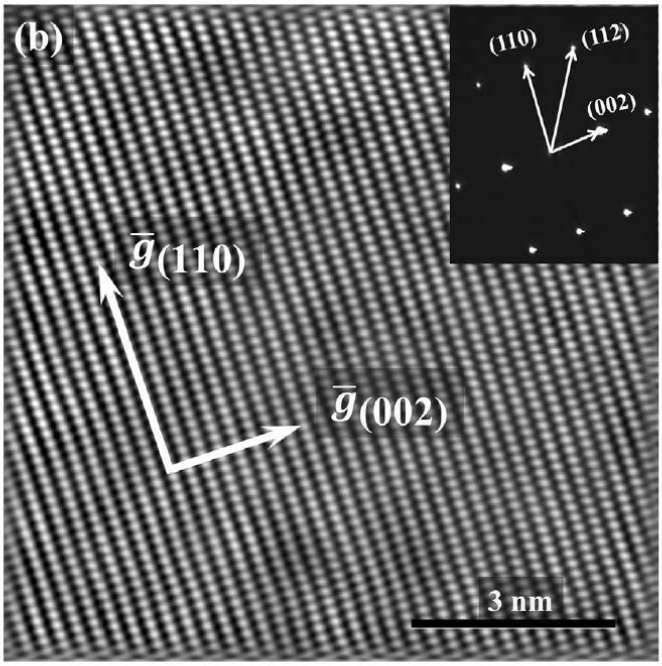

Fig. 6. HRTEM micrographs of a nanorod of sample TZ3. a) Single crystal, columnar morphology of the nanorod and lattice fringes consistent with (002) family planes; inset shows a general view of the nanorod. b) Fast Fourier transform processing of the squared region signaled in (a), disposition of lattice fringes transversal and parallel to the axial direction of the nanorod; inset corresponding SAED pattern.

Previous reports working with the spray pyrolysis technique (for which the experimental configuration is close to that of the AACVD) summarized the synthesis of ZnO nanorods as a function of different deposition times and crystalline substrates [5–7,12]. These authors concluded that using extended deposition periods, the development of a uniform layer of material was reached, in agreement with the present work. As expected, this outcome can be attributed to the continuous delivery of reactants at the surface vicinity. Additionally to this observation, another crucial factor influencing the homogeneity of the material resulted fromthe use of a polycrystalline layer (TiO_2) previously grown on the substrate instead of using bare glass. This outcome suggests that the formation of nucleation centers was evenly distributed in the

oxide surface. This effect was also in accordance to the previous observations reported elsewhere [2,4,6–8,10,12].

Optical properties: Total transmittance and reflectance spectra of sample TZ3 appear in Fig. 7(a). Low transmittance and reflectance values were observed in the UV region (b400 nm), which corresponds to the borosilicate glass substrate and bi-layer (TiO_2 and ZnO nanorods) absorption. In addition, sample TZ3 showed significant reflectance behavior (~45%) at about 400 nm, followed by a gradual decrease as the wavelength increases. The origin of this characteristic is not well explained in terms of observed microstructure or surface topography.

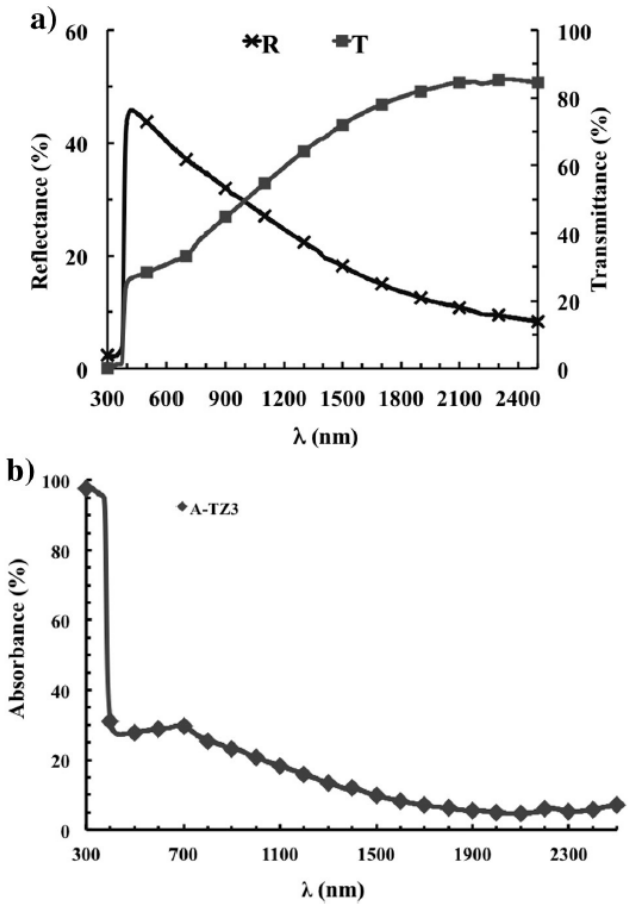

Fig. 7. Optical properties of sample TZ3. a) Transmittance–reflectance and b) absorbance spectra.

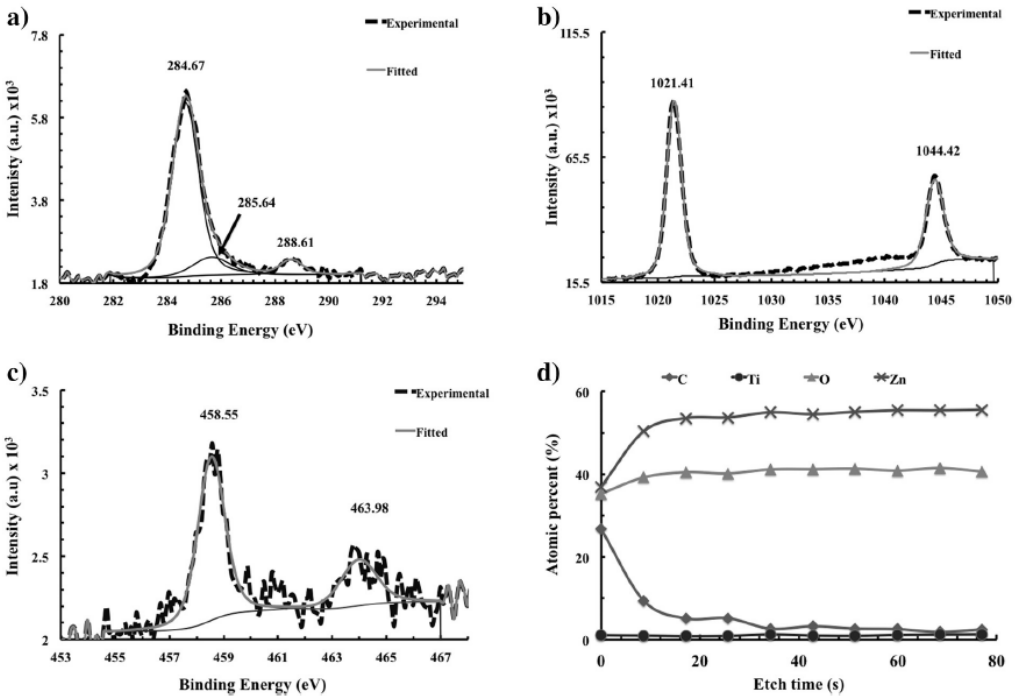

Fig. 8. Individual XPS spectra for detected elements in sample TZ3. Figures correspond to: a) C1s, b) Zn2p and c) Ti2p and d) element distribution (at%) in depth analysis performed for sample TZ3.

The tendency of gradual increase of transmittance and decrease of reflectance in VIS and NIR regions, was related to the usual decrease of refractive index as wavelength increases, for all the materials involved (ZnO, TiO_2 and borosilicate glass). Absorbance spectra for sample TZ3, obtained from transmittance and reflectance measurements, appears in Fig. 7(b). A high absorbance in the UV region followed by a sharp decrease at around 400 nm can be observed, as a consequence to the borosilicate substrate and bi-layer absorption. An evident absorption region in the VIS interval, can be associated to the rough topography of its surface producing a trapping of incident light.

Chemical composition analysis: The core level spectra in Fig. 8 for C1s, Zn2p and Ti2p regions by means of XPS, were collected from sample TZ3. The presence of C as shown in Fig. 8(a) was visible only at the top surface and resulted from

environmental contamination due to carbonate species such C\O, C_O or C\C [25]. Spectra for Zn2p in Fig. 8(b) exhibited two distinctive peaks at 1021.41 and 1044.42 eV, which along to O1s peak at 530.17 eV (not shown), corresponded to the characteristic signal of ZnO. Analysis of Ti2p spectra in Fig. 8(c) showed the presence of peaks at 458.55 and 468.83 eV defining the presence of TiO_2 [25]. Even though TiO_2 was detected as a sample's component, this result was not an indication of its presence at surface but instead, the signal came from information at the bottom of the nanorods (thin film layer) that could resulted from empty spaces within the analyzed region of the sample. A confirmation of this observation was obtained from the stoichiometric distribution of the elements (at.%) in depth analysis as shown in Fig. 8(d), from were the Zn2p and O1s signals were much more visible than Ti2p and C1s, behavior that was well maintained in the profundity.

Conclusions:

ZnO nanorods on TiO_2 film covered borosilicate substrates were deposited by AACVD technique. Nanorods were single-crystals with welldefined hexagonal prismmorphology,with its longitudinal axis parallel to the reciprocal lattice vector $g_{(002)}$ and transversal direction parallel to $g_{(110)}$. The development of a uniformand compactness deposit of nanorods was achieved by employing the lowest scan velocity of the nozzle. For optimized sample, a full texture analysis was possible and used to determinemore accurately the mean growth direction of the nanorods, which appeared having its [001] direction distributed close to the normal of substrate surface, with an angular spread of 20° ± 2°. This fact was consistent with SEM analysis of average nanorod axis inclination around substrate normal of−4°±23°. These results proved

thatwithin the combination of 2D X-ray diffraction methods and computational modeling, a reliable and proper texture definition can be determined.

Acknowledgments:

The authors thank E. Torres-Moye, O. Solis-Canto, S. Miranda, K. Campos-Venegas and C. Leyva-Porras for the technical support. In addition, the authors also thank the Stanford Synchrotron Radiation Laboratory, a national user facility operated by Stanford University on behalf of the U.S. Department of Energy, the Office of Basic Energy Sciences (proposal No. 3939) and the CONACYT (grant number 106655), for the partial financial support provided for the development of this project.

References:

[1] D. Ariosa, F. Elhordoy, E.A. Dalchiele, R.E. Marotti, C. Stari, Texture vs morphology in ZnO nano-rods: on the X-ray diffraction characterization of electrochemically grown samples, J. Appl. Phys. 110 (2011) 124901–124909.

[2] Y.J. Kim, H.M. Shang, G.Z. Cao, Growth and characterization of [001] ZnO nanorod array on ITO substrate with electric field assisted nucleation, J. Sol-Gel Sci. Technol. 38 (2006) 79–84.

[3] E. Kärber, T. Raadik, T. Dedova, J. Krustok, A. Mere, V. Mikli, M. Krunks, Photoluminescence of spray pyrolysis deposited ZnO nanorods, Nanoscale Res. Lett. 6 (2011) 359–366.

[4] J. Qiu, X. Li,W. He, S.-J. Park, H.-K. Kim, Y.-H. Hwang, H.-J. Lee, Y.D. Kim, The growth mechanism and optical properties of ultralong ZnO nanorod arrays with a high aspect ratio by a preheating hydrothermal method, Nanotechnology 20 (2009) 155603–155612.

[5] C.Y. Dwivedi, V. Dutta, Vertically aligned ZnO nanorods via self-assembled spray pyrolyzed nanoparticles for dye-sensitized solar cells, Adv. Nat. Sci. Nanosci. Nanotechnol. 3 (2012) 015011–015019.

[6] T. Dedova, O. Volobujeva, J. Klauson, A.Mere,M. Krunks, A novel deposition method to grow ZnO nanorods: spray pyrolysis, Superlattice. Microst. 42 (2007) 444–450.

[7] T. Dedova, I. Oja Acik, M. Krunks, V.Mikli, O. Volobujeva, A. Mere, Effect of substrate morphology on the nucleation and growth of ZnO nanorods prepared by spray pyrolysis, Thin Solid Films 520 (2012) 4650–4653.

[8] T. Dedova, O. Volobujeva, M. Krunks, V. Mikli, I. Gromyko, A. Katerski, A. Mere, Growth of ZnO rods on FTO electrodes by spray pyrolysis, Mater. Sci. Eng. 49 (2013) 012001–012005.

[9] F. Solís-Pomar, E. Martínez, M.F. Meléndrez, E. Pérez-Tijerina, Growth of vertically aligned ZnO nanorods using textured ZnO films, Nanoscale Res. Lett. 6 (2011) 524–535.

[10] S. Xu, Z.L. Wang, One-dimensional ZnO nanostructures: solution growth and functional properties, Nano Res. 4 (2011) 1013–1098.

[11] X. Li, J. Wang, J. Yang, J. Lang, S. Lü, M. Wei, X. Meng, C. Kou, X. Li, Comparison of photocatalytic activity of ZnO rod arrays with various diameter sizes and orientation, J. Alloys Compd. 580 (2013) 205–210.

[12] M. Krunks, T. Dedova, I. Oja Açik, Spray pyrolysis deposition of zinc oxide nanostructured layers, Thin Solid Films 515 (2006) 1157–1160.

[13] R.S. Devan, R.A. Patil, J.-H. Lin, Y.-R. Ma, One-dimensional metal-oxide nanostructures: recent developments in synthesis, characterization, and applications, Adv. Funct. Mater. 22 (2012) 3326–3370.

[14] B.R. Mehta, F.E. Kruis, A graded diameter and oriented nanorod-thin film structure for solar cell application: a device proposal, Sol. Energy Mater. Sol. Cells 85 (2005) 107–113.

[15] K.H. Brosnan, G.L. Messing, R.J. Meyer, M.D. Vaudin, Texture measurements in b001N fiber-oriented PMN–PT, J. Am. Ceram. Soc. 89 (6) (2006) 1965–1971.

[16] P. Amézaga-Madrid, W. Antúnez-Flores, J.E. Ledezma-Sillas, J.G. Murillo-Ramírez, O. Solís-Canto, O.E. Vega-Becerra, R. Martínez-Sánchez, M. Miki-Yoshida, Microstructural properties of multi-nano-layered YSZ thin films, J. Alloys Compd. 509S (2011) S490–S495.

[17] A. Sáenz-Trevizo, P. Amézaga-Madrid, P. Pizá-Ruíz, O. Solís-Canto, C. Ornelas-Gutiérez, S. Pérez-García, M. Miki-Yoshida, Microstructural characterization, optical and photocatalytic properties of bilayered CuO and ZnO based thin films, J. Alloys Compd. 615 (1) (2014) S375–S381.

[18] A.P. Hammersley, S.O. Svensson, M. Hanfland, A.N. Fitch, D. Hausermann, Twodimensional detector software: from real detector to idealised image or two-theta scan, High Press. Res. 14 (1996) 235–248.

[19] http://cimav.edu.mx/investigacion/software/anaelu (Updated: October 19, 2010).

[20] L. Fuentes-Montero, M.E. Montero-Cabrera, L. Fuentes-Cóbas, The software package ANAELU for X-ray diffraction analysis using two-dimensional patterns, J. Appl. Crystallogr. 44 (2011) 241–246.

[21] ICDD XRD Database PDF Number 00-021-1272, 1990.

[22] ICDD XRD Database PDF Number 01-075-1533, 1997.

[23] Swee-Yong Pung, Kwang-Leong Choy, Xianghui Hou, Chongxin Shan, Preferential growth of ZnO thin films by the atomic layer deposition technique, Nanotechnology 19 (2008) 435609–435616.

[24] J. Ramos-Cano, A. Hurtado-Macías,W. Antúnez-Flores, L. Fuentes-Cobas, J. González-Hernández, P. Amézaga-Madrid, M. Miki-Yoshida, Synthesis by aerosol assisted chemical vapor deposition and microstructural characterization of PbTiO3 thin films, Thin Solid Films 531 (2013) 179–184.

[25] C.D. Wagner, W.M. Riggs, L.E. Davis, J.F. Moulder, G.E. Muilenberg, Handbook of X-ray Photoelectron Spectroscopy, Perkin-Elmer Corporation, Eden Prairie, Minnesota, 1979. 40–89.